Dynamic polarity of curved aromatic soot precursors

Jacob W. Martin[a,b], Angiras Menon[a,b], Chung Ting Lao[a], Jethro Akroyd[a], Markus Kraft*[a,b,c,]

[a]*Department of Chemical Engineering and Biotechnology, University of Cambridge, Philippa Fawcett Drive, West Site, CB3 0AS Cambridge, UK*
[b]*Cambridge Centre for Advanced Research and Education in Singapore (CARES), CREATE Tower, 1 Create Way, Singapore 138602*
[c]*School of Chemical and Biomedical Engineering, Nanyang Technological University, 62 Nanyang Drive, Singapore 637459*

Abstract

In this paper, we answer the question of whether polar curved aromatics are persistently polar at flame temperatures. We find, using electronic structure calculations and transition state theory, that the inversion barriers of curved aromatics (cPAH) of 0.9–1.2 nm in diameter are high and that they are not able to invert over the timescales and at the high temperatures found in sooting flames. We find a transition for smaller curved aromatics between 11–15 ($\approx$ 0.8 nm) rings where the increasing strain introduced from the pentagonal ring increases the inversion barrier leading to rigidity. We then performed *ab initio* quantum molecular dynamics to find the molecular dipole fluctuations of a nanometre sized cPAH at 1500 K. We found the bending mode of the bowl shaped molecule gave rise to the largest fluctuations on the dipole moment by $\pm$0.5–1 debye about the equilibrium value of 5.00 debye, indicating persistent polarity. We also observed binding of a chemi-ion at 1500 K over 2 ps, suggesting the molecular dipole of cPAH will be an important consideration in soot formation mechanisms.

Keywords: soot formation, ion-induced nucleation, curved PAH inversion, buckybowl, curved PAH, polar aromatics, fullerene-like

Email address: mk306@cam.ac.uk (Markus Kraft*)

1. Introduction

The transformation of gas phase aromatic precursors to solid soot nanoparticles remains the most challenging aspect of soot formation [1]. The rapid second order dynamics of soot formation [2, 3] and the observation of stack mode in mass spectrometry [4, 5] suggest a physical aggregation process. The estimated size of the pericondensed aromatics in early soot nanoparticulates is 0.9–1.2 nm from optical band gap measurements [6, 7, 8], Raman spectroscopy [6, 9] and laser desorption ionisation time of flight mass spectrometry [10, 11]. However, to date, rapid physical aggregation of planar polycyclic aromatic hydrocarbons (PAHs) of this size has lacked the significant interaction energies required to be stable at the flame temperatures in which soot nanoparticles form [1, 12, 13].

Aromatics that are curved due to pentagon integration have long been suggested as a precursor for soot formation [14, 15]. A small curved PAH (hereafter referred to as cPAH), corannulene (structure **1** in Figure 1) , has been extracted from soot [16, 17] and the synthesis of closed cage fullerenes molecules in low pressure benzene flames have been observed [18, 19]. High resolution transmission electron micrographs have been used to suggest curvature in soot and carbon black from bent fringes [20, 21] with fringe analysis recently being used to quantify the amount (>62.5%) and degree of curvature of aromatics (1–3 pentagonal rings) in early soot particles [7, 22, 23, 24]. Curvature was suggested to be integrated through the HACA mechanism with acetylene addition to an armchair site containing a pentagonal ring [25, 26, 27, 28, 29] or oxidation of a zig zag site [30] as well as by crosslinks that rearrange into curved pericondensed structures containing internal pentagonal rings [14, 15].

At the recent 37$^{\text{th}}$ International Symposium on Combustion, we suggested the importance of considering the significant polarity of these cPAH species [31]. Our detailed electronic structure calculations revealed a significant electric polarisation that occurs at the strained integrated pentagons in curved PAH due to the flexoelectric effect (4–6 debye for species found in early soot) [32, 23]. Further calculations suggested that the dimerisation energy of cPAHs with 1–2 pentagons were found to be comparable to that of similar sized planar PAHs. The calculations also suggested that for a PAH to become flexoelectric more than six aromatic rings are required. Electrostatic interactions between permanent dipoles range significantly farther than dispersion interactions, suggesting an influence on the stability of early soot

clusters [31].

The interaction of cPAHs with charged species in flames is of particular interest. We calculated significant binding energies between cPAH and the dominant chemi-ion in sooting hydrocarbon flames, cyclopropenyl ($C_3H_3^+$) (>40 kcal/mol [23]). Chemi-ions are produced in significant concentrations in flames and their correlations with soot formation have long been known [33, 34, 35, 36], such as the impact of electric fields [37, 38, 39] and the addition of alkali metal ions [40, 41, 42]. Recently, Carbone et al. [43, 5] found that atmospherically sampled cations from a flat flame formed nanometre sized positive clusters through physical aggregation of pericondensed aromatics, while negative ions did not readily grow into nanoparticles, further indicating a charge dependent growth mechanism is possible.

One significant issue raised at the symposium surrounding such an ionic route was how persistent the polarity of curved PAH is at the temperatures of sooting flames. Dynamic polarity presents two problems for interactions of cPAH with each other and chemi-ions: 1) rapid inversions of cPAH would likely impede their ability to form a stably bound complex, 2) fluctuations of the dipole moment at flame temperatures could mean that the dipole moment decreases, thereby preventing the formation of a cPAH cluster. For inversion the small cPAH corannulene is well known to rapidly invert at room temperature with an experimental inversion barrier of 10.2 kcal/mol [44] and computed barrier of 11.5 kcal/mol [45]. This barrier is significantly lower than the strain energy anticipated in corannulene 24 kcal/mol [46], this lower inversion barrier was explained by the planar transition state that increases π-electron delocalisation decreasing the barrier by 11 kcal/mol [47]. Soon after corannulene was found to invert rapidly at room temperature it was also found that by addition of a single extra pentagonal ring about the rim, the inversion barrier was doubled and the inversion was halted at room temperature [48]. Calculations of larger cPAH have found a non-planar S-shaped transition state that considerably increases the inversion barrier with a one pentagon 10 ring species giving an inversion barrier of 56 kcal/mol while two pentagon >14 ring species gave inversion barriers of >100 kcal/mol [49].

In this paper, we aim to determine the persistence of cPAHs polarity at temperatures at which soot forms in a flame and study the interaction of an ion with a dipolar cPAH. The rate of inversion is computed for a range of cPAH revealing the size required for inhibition of inversion in flame conditions. We then use *ab initio* molecular dynamics simulations to track the fluctuation of the dipole moment of a cPAH and study the dynamics of

a chemi-ion interacting with the cPAH over two picoseconds.

2. Methodology

Figure 1 shows the curved PAHs chosen for this study. These include the smallest aromatic, curved by pentagon integration that we have found, corannulene **1** [31]. We then considered molecules of the size seen in early soot particles 0.9–1.2 nm; a fifteen ring structure with a single pentagonal ring and a five member bay site **2**, the same single pentagon structure with the closure of the bay site **3**, a two pentagon containing 15 ring cPAH **4** suggested from HRTEM imaging of early soot nanoparticles [23], a three pentagon containing cPAH is also provided **5**. For each of the largest cPAH we also added/removed a hydrogen to the site specified to consider the effect of a π-radical on the rate of inversion.

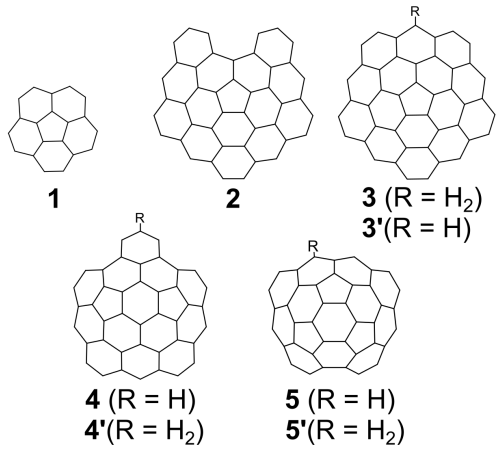

Figure 1: Curved PAH molecules chosen in this study with **3**–**5** chosen from a previous study [23].

The energies and frequencies of the minimum energy and transition state structures of the curved PAHs were computed using the hybrid density functional B3LYP/6-311+G(d,p) level of theory. This has been found to correctly describe the equilibrium geometry of curved arenes compared with crystal structures and the inversion dynamics of these systems [49]. For all geometries located by DFT, the frequencies were checked to ensure the calculation had found the appropriate minima and transition states. To obtain a more

accurate estimate of the energies of the minima and the transition state, single point energy calculations using the Minnesota hybrid density functional M06-2X/6-311g(d,p) were performed on the optimised geometries. This has been shown to give accurate energies for reactions involving PAHs [50]. Energies are reported with the zero point energy correction included.

The rate of inversion was calculated using canonical transition state theory as implemented within the THERMO package of the Multiwell software [51, 52, 53]. In this case the barriers of inversion are high and pressure dependence was not considered, so canonical transition state theory was considered sufficient over more sophisticated methods such as variational transition state theory and RRKM/Master Equation calculations. Due to the larger size of the 15 ring PAHs, the source code had to be modified to include more vibrational and rotational degrees of freedom than the default 150 implemented in Multiwell. Additionally, tunneling was not treated by the standard unsymmetrical Eckart tunneling in THERMO as the very large barriers of inversion led to some numerical difficulties with this tunneling form. Instead, tunneling effects were treated by means of the Wigner correction. For the rate calculations in this work, the obtained Wigner tunneling corrections were extremely close to one, which is expected given the large reactants and high energy barriers.

Ab initio molecular dynamics (AIMD) techniques were used to study the thermal fluctuation of the cPAH. These methods have been used previously in combustion to study the dimer lifetimes of pyrene using a semi-empirical quantum theory. In Born-Oppenhiemer molecular dynamics (BOMD) nuclei are approximated as classical ions with the forces on these ions computed from the electronic structure,

$$\partial E/\partial \mathbf{R} = \langle \Psi | \partial H/\partial \mathbf{R} | \Psi \rangle + \langle \partial \Psi/\partial \mathbf{R} | H | \Psi \rangle + \langle \Psi | H | \partial \Psi/\partial \mathbf{R} \rangle \,, \qquad (1)$$

with the first term being the Hellmann-Feynman force and the second and third term being the "Pulay" forces [54]. BOMD performs a self-consistent field calculation to iteratively determine the electronic structure at each time step, which is prohibitively expensive. One successful approximation is ADMP that propagates the electronic structure using an extended Lagrangian coupled to the nuclear positions via a fictitious mass, which significantly reduces the computational cost of such calculations. This is similar to the Car-Parrinello method, however for ADMP, the density matrix is propagated instead of the Kohn-Sham orbitals and atom-centred Gaussian basis

functions are used instead of plane wave basis functions [54]. These features of ADMP allow any hybrid density functional theory to be used to generate the density matrix and provides a better separation between the electronic and nuclear degrees of freedom. With small timesteps (<0.5 fs) it has been found to accurately follow the fully converge Born-Oppenheimer MD with vibrations and energy being independent of the fictitious mass used [54, 55, 56, 57]. Since it was implemented in Gaussian 03 it has seen applications in describing gas interactions with aromatic macrocycles [58] and recently been used to model the formation of covalent bonds between pyrene dimers [59]. A similar method using converged semi-empirical PM3 simulations has also been employed in combustion research to study PAH dimerisation at flame temperatures by Schuetz and Frenklach [60], Wong et al. [61].

For the AIMD simulation used in this study a more economic level of theory, B97D/6-31G(d), was used. The hybrid density functional theory with dispersion correction B97D [62] has performed well compared with benchmark coupled cluster calculations for cation-benzene clusters and dimers of corannulene (error <1 kcal/mol B97D/cc-pVTZ) [63, 64, 31]. For the molecular system **4** a dipole moment of 5.00 debye was calculated, which is slighty below (<4%) the value calculated at a higher level of theory 5.32 debye [23]. We calculated binding energies of 40.9 kcal/mol, which is larger than that calculated at a higher level of theory B97D/cc-pVTZ = 38.1 kcal/mol but should provide preliminary insight into the dynamics of the system [23]. In simulating the $C_3H_3^+$ -**4** system we found little impact of the fictitious mass on the energetics, as others have also documented [56] and therefore we made use of the default mass of 100 amu. We used a timestep of 0.1 fs to ensure energy conservation during the simulation. A NVT ensemble was enforced to maintain the high temperatures found within the flame where soot forms (1500 K). Ergodicity was confirmed after the first ≈300 fs by computing the velocity-velocity autocorrelation function. Dynamics were only recorded after this initial thermalisation had been performed. No angular momentum was included in the system to provide a better understanding on the vibrational degrees of freedom. Gaussian 16 was used for all of the electronic structure and AIMD calculations performed in this work [65].

3. Results and discussion

3.1. Inversion of curved PAH at flame temperatures/timescales

To introduce the inversion process we have plotted the energies and geometries of the transition state for inversion of molecules **1**, **2** and **3** (Figure 2). For the smallest structure corannulene **1** the barrier was low, 11 kcal/mol, due to the planar transition state as discussed earlier. Enlarging the PAH so that it was similar in size to those found in soot **2** increases the inversion barrier considerably, raising it to 59 kcal/mol. The transition state was still found to be planar for this geometry.

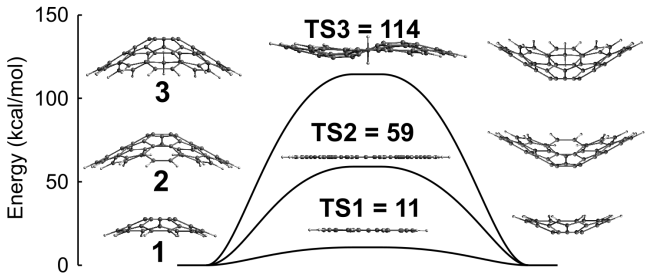

Figure 2: Energies and geometries of the inversion transition states.

Figure 3 shows the bond lengths of the equilibrium geometry and the transition state showing the considerable strain in the system. The first thing noticed was the reduction in bond lengths at the pentagonal site. For the bay site we see the considerable increase in the distance between the bay exterior carbons, 3.3 Å to 3.92 Å and a lengthening of the bonds around the baysite 1.5 Å to 1.58 Å. This flattening expands the exterior rings and compresses the interior carbon network and is consistent with strain from the σ-bonding - skeleton strain.

Closing the bay site of **2** to form species **3** gives rise to an almost doubling of the inversion barrier. Figure 2 shows the S-shaped transition state formed due to this bay closure. It is important to note that for the S-shaped transition state the inversion still involves all core carbon atoms flipping from one side to the other. Figure 4 shows the imaginary frequency associated with the planar transition state for **2** and the S-shaped transition state for **3**. The main difference in the transition state being the warped nature of **TS3**.

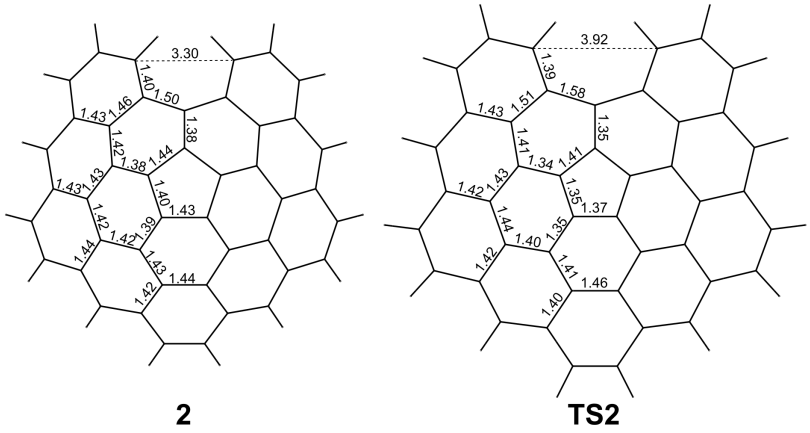

Figure 3: Geometries of molecule **2** at equilibrium and at the transition state **TS2**.

This warping indicates the skeletal strain overcomes the π-bonding to produce the S-shape. We have previously found a similar interplay of curvature vs planarity with small pentagon containing PAH [31].

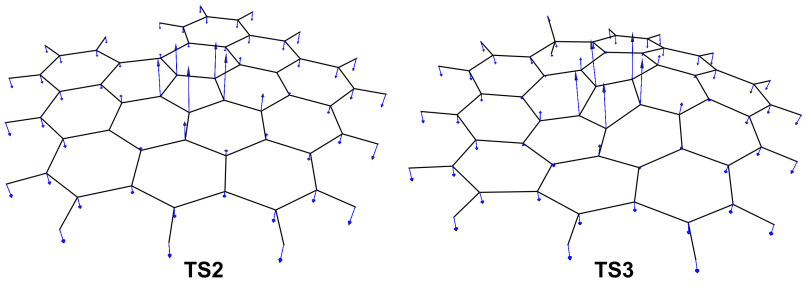

Figure 4: Molecular geometries with blue arrows indicating the relative amplitude and direction of the imaginary vibrations associated with the transition states of molecules **2** and **3**.

Increasing the number of pentagons increases the barrier to inversion. Figure 5 shows the transition state energies and geometries for cPAH containing one **3**, two **4** and three **5** pentagonal rings. A modest increase is seen between one and two pentagonal rings, 114 to 138 kcal/mol, respectively. Integration of three pentagonal rings significantly increases the inversion barrier with molecule **5** barrier rising to 360 kcal/mol. The transition state geometries are heavily pyramisalised and warped with no internal carbon atoms being completely planar, thus significantly disrupting the π-bonding.

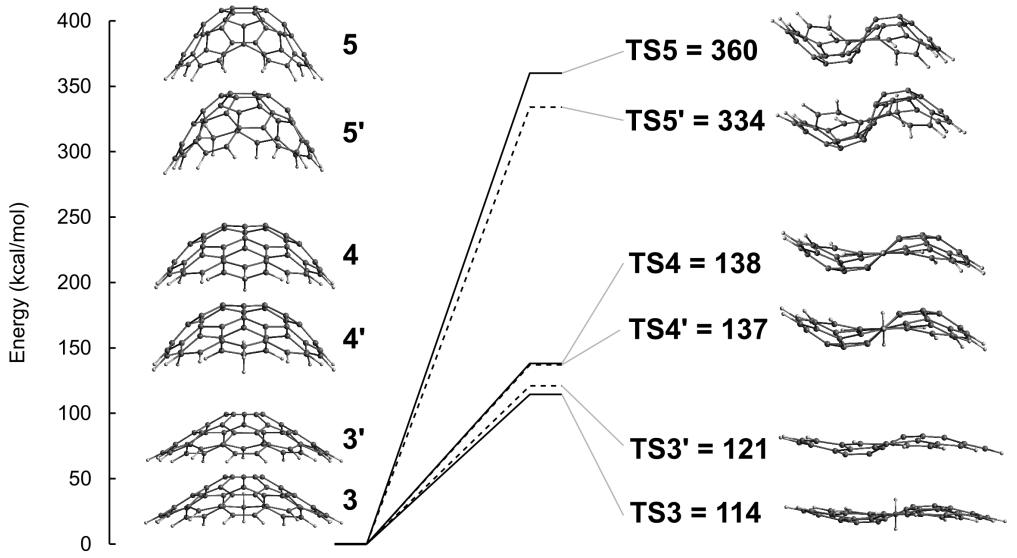

Figure 5: Inversion barriers and molecular geometries for molecules **3**, **4** and **5** as well as their π-radicals **3'**, **4'** and **5'** dashed line.

Minimal changes in the inversion barrier was seen for the π radicals compared with the closed shell structures. In the case of **TS3'** we even saw an increase in the barrier to inversion. We think this is due to the loss of hydrogen leading to an increased aromaticity and therefore stability of the transition state. This suggests that the aromaticity is more important than the π radical nature for transition states near planarity. Little change was seen for the two pentagon containing molecule's transition state **TS4/TS4'**. The most strained structure has the most significant radical effect **5** decreasing the barrier for inversion by 26 kcal/mol.

The geometries and frequencies calculated were used to compute the inversion rate for the species in Figure 1. The reciprocal of the inversion rate constant was used, $1/k = \tau$, which can be thought of as a characteristic time for inversion, as a function of the temperature. The characteristic time can be compared to the time scale of soot formation, which in a premixed flame is from micro to milliseconds [3]. Any characteristic time below a millisecond will then be important for early soot formation as above this value no inversion can occur on the time scale of soot formation. Another distinction can be made considering the temperature in the flame where soot forms which are near 1500 K [1]. Figure 6 shows that only corannulene has considerable

low temperature inversion **1**, which is a well known result experimentally verified by Scott et al. [44]. Molecule **2** is able to invert at high temperatures, however, for the other molecules and their radicals the temperature required for them to invert during soot formation timescales is too high that the molecules would breakdown before this threshold was reached.

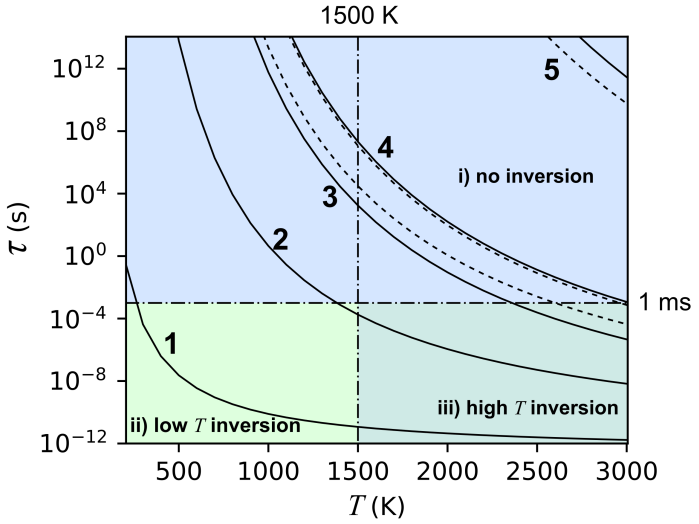

Figure 6: Characteristic time for inversion for the species shown in Figure 1 with π-radicals shown in dashed line.

Table 1: Inversion barriers E_{inv} (kcal/mol), values from the Arrhenius fitting of the form $k = A\exp(-E_a/k_bT)$ (s^{-1} and kcal/mol), the rate of inversion at 1500 K (cm^3 mol^{-1} s^{-1}) and the characteristic time, $\tau = 1/k$, at 1500 K (s).

Species	E_{inv}	A	E_a	Rate at 1500 K	τ at 1500 K
1	11	3.76×10^{12}	11.2	8.62×10^{10}	11.6 ps
2	59	3.10×10^{12}	60.0	5.62×10^{3}	180 μs
3	114	5.64×10^{13}	116.5	5.76×10^{-4}	1737 s
3'	121	1.70×10^{13}	121.6	3.28×10^{-5}	30.5×10^{3} s
4	138	1.09×10^{13}	139.6	4.74×10^{-8}	21.1×10^{6} s
4'	137	1.47×10^{13}	138.7	8.65×10^{-8}	11.6×10^{6} s
5	360	1.32×10^{15}	365.5	6.82×10^{-39}	0.15×10^{39} s
5'	334	8.07×10^{14}	339.3	2.69×10^{-35}	36.2×10^{33} s

In order to extend this analysis to consider the onset of rigidity in smaller

curved PAH we have considered the size dependency of the inversion. This was achieved by using the exponential relationship between the characteristic time and the barrier for inversion calculated for the species in Figure 1, to determine a barrier of 66.3 kcal/mol that would provide a characterisitic time of 1 millisecond at 1500 K. This allows us to consider the inversion barrier's previously calculated by others at similar levels of theory [66, 67] to provide a clear picture for when inversion will be halted at flame temperatures/timescales of interest. Figure 7 shows the inversion barrier for different species as a function of the total number of hexagonal and pentagonal rings (from our previous study of Gaussian curvature and the integration of curvature [68, 31] we defined pentagons as an internal pentagon surrounded by 5 hexagonal rings or an exterior pentagon that has >3 neighbouring hexagonal rings that are adjacent to each other).

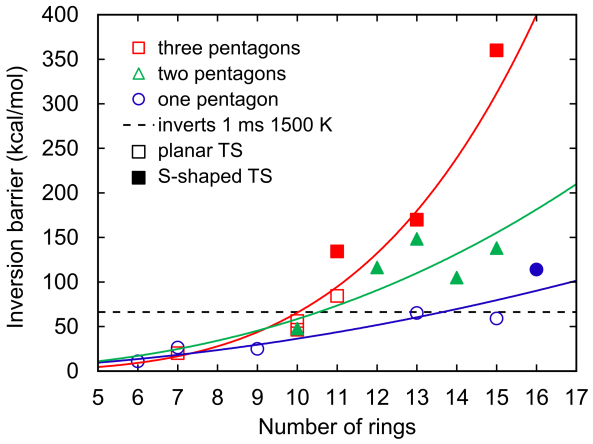

Figure 7: Inversion barrier as a function of the number of rings for structures in this work and from previously studied cPAH [66, 67]. The dashed line highlights the inversion barrier 66.3 kcal/mol which provides a characteristic time of 1 ms at 1500 K from our calculations.

Three different size ranges were found for the inversion behaviour of peri-condensed cPAH. For $6 \leq N_{rings} < 11$ inversion occurs rapidly at flame temperature. For $11 \leq N_{rings} \leq 15$ inversion does not occur for species with $\geq$2 pentagonal rings but is possible for species containing a single pentagonal ring. For $15 < N_{rings}$ structures are stability curved during the entirety of soot formation.

Considering the impact of inversion on soot formation a few conclusions

can be drawn. For small curved PAH we expect that inversion is an important consideration with corannulene inverting rapidly, which will average out the flexoelectric dipolar effect. This is somewhat seen in the similar vapour pressure of perylene and corannulene [69]. Addition of rings increases the inversion barrier so that for the size of PAH seen in early soot particles the inversion is not rapid enough to be important at flame temperatures and timescales. The π-radical nature does not significantly lower the barrier for inversion indicating the skeletal strain dictates the inversion dynamics.

Further work is needed to understand the rate of inversion of cPAH inside clusters as barriers for inversion of cPAH have been found to decrease in the presence of a planar PAH [70, 71] or in different molecular environments [72]. These effects only operate for cPAH with planar transition states. It appears that the transition from planar to S-shaped transition states determines when the cPAH becomes rigid at flame temperatures. This can be seen in Figure 7 where the larger barriers for inversion are predominately for those species with S-shaped transition states (denoted by filled symbols).

While it seems unlikely inversion will occur for cPAH found in early soot particles the suggestion of an interaction with a chemi-ion needs to be considered to see if it can catalyse an inversion. This will be considered for molecule **4** in the presence of $C_3H_3^+$. Figure 8 shows the barrier for inversion, which was lowest when going from the convex arrangement to the transition state **4+(**. The transition state energy barrier was similar, 140 kcal/mol, compared to without an ion, 138 kcal/mol, indicating the presence of the ion has a minimal effect on the inversion barrier and therefore the dynamics of the bowl.

3.2. Fluctuations of the dipole moment

In order to consider the fluctuations of the dipole moment of a cPAH at temperatures in the flame where soot inception occurs we have performed AIMD simulations. Due to the expense of the calculations we decided to include a chemi-ion, which allows for some insights to be gained on the impact of cPAH flexoelectric dipole at high temperatures and as the inversion dynamics are minmimally impacted by the chemi-ion we can consider the cPAH fluctations as being independent. The chemi-ion was placed on the top surface of the bowl as this is the expected binding site for an ion approaching from a large distance with the flexoelectric dipole aligning to interact with the positive charge. The simulation was run for half a picosecond in order

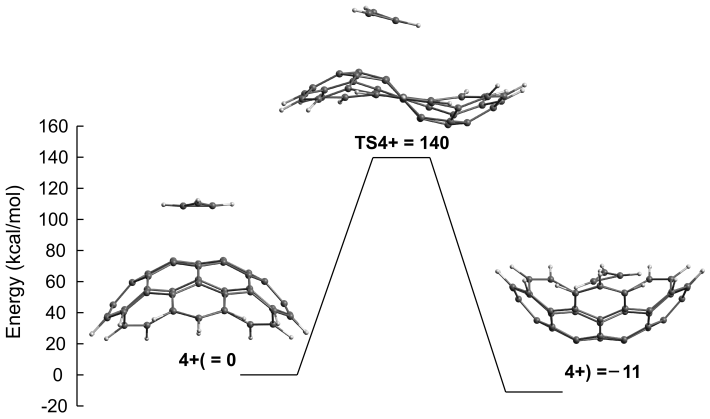

Figure 8: Barrier for inversion for molecule **4** in the presence of an ion.

for the thermal energy to equilibrate and stabilise after which the dynamics of molecule **4** and the chemi-ion $C_3H_3^+$, **4+(**, were followed over 2 ps.

Figure 9 a shows the trajectory of the atomic positions over the first picosecond. Concentrating on the cPAH fluctuations we see that the carbon atoms near the middle of the aromatic plane had a reduced range of motion compared to the atoms around the rim of the cPAH. The main low frequency vibrations observed were bending mode vibrations where the edge warps. This bending modes occurred with a frequency of 250–350 fs. The local flexoelectric dipole moment changed with this vibration. Instead of calculating the dipole moment at every time step, which would have been prohibitively slow, geometries were chosen over one of these bending modes and single point energy calculations performed of the cPAH only (Figure 9b). The dipole moment at this level of theory was 5.00 D and therefore the dipole moment was found to fluctuate by ±0.5–1.0 debye, ±10–20%. This analysis showed that at temperatures in the flame where soot forms large cPAH have a persistent polarity that does not decrease substantially during thermal excitation.

The movement of the chemi-ion was then considered in the presence of the cPAH. While the ground state equilibrium geometry shows a binding site above the pyramidalised carbon atoms the chemi-ion was found to move freely across the surface from the top of the bowl to the edge of the bowl. Figure 9a shows the chemi-ion trapped at the rim of the cPAH for the first picosecond. From the electrostatics we can explain the edge binding as being

due to the charge concentration at the edge of the PAH from the induced dipole on the rim carbon atom caused from the C–H bond [73] and the binding to the pyramidalised atoms due to the flexoelectric dipole moment [32]. The binding of the chemi-ion does not appear to be influenced strongly by the bending mode of the cPAH as seen in Figure 9b. Figure 9c shows the movement of the chemi-ion across the top surface of the cPAH interacting with the pentagonal carbon atoms where the flexoelectric effect is greatest.

Further work is required on the dynamics of cPAH ion system. We only considered one cPAH chemi-ion pair, however, there are innumerable other combinations, some of which are worth considering in detail, such as the CHO+ cPAH combinations and considering smaller cPAH. We suggest that the main conclusions about dipole fluctuations we have found with molecule **4** hold for all cPAH with a large inversion barrier (>66 kcal/mol). For other ionic interactions, e.g. CHO^{+}, have the potential to interact more strongly

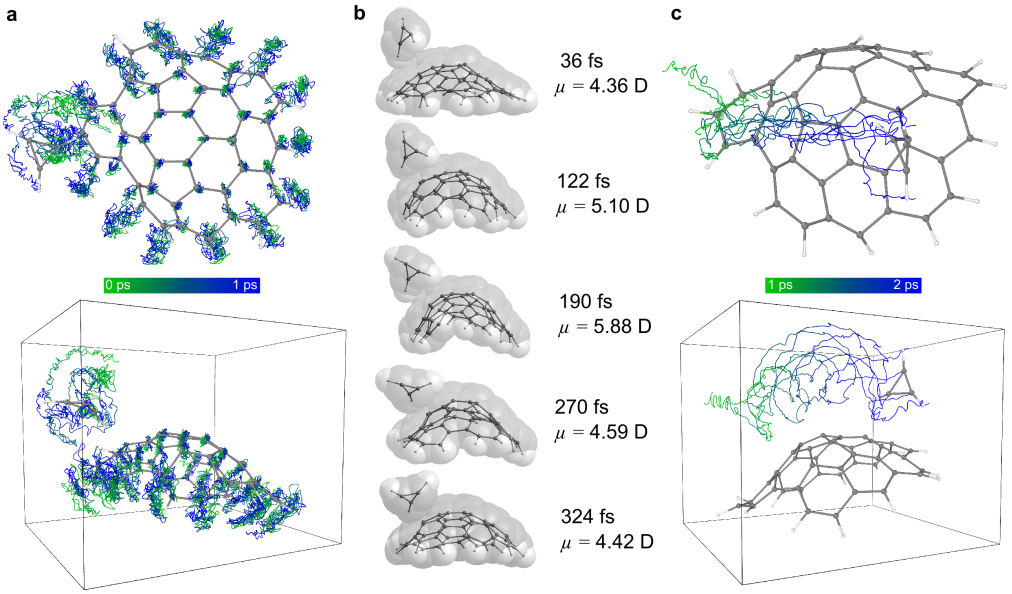

Figure 9: Dynamics of molecule **4** and the chemi-ion. a) dynamics of the complex over the first picosecond shown with a line at each atom with the geometry at 1 ps shown with a ball and stick model. b) Fluctuation of the bowl during a low frequency bending model vibration. The dipole moment was calculated for the bowl fragment. c) dynamics of the complex over the second picosecond with the geometry shown with the ball and stick model for the final structure at 2 ps.

than $C_3H_3^+$ [13]. Additionally, as our study of chemi-ion-cPAH interactions does not capture long term dynamics for accurate statistics of the chemi-ion cPAH system we are working on developing less costly descriptions to study longer dynamics. We also did not consider the impact of rotational degrees of freedom in order for the cPAH fluctuations to be more clearly observed but this is expected to improve the binding tendencies as studies have previously found for planar PAH homodimers [60, 61]. The movement of the chemi-ion across the surface of the bowl and rim provides an opportunity for reactions with the rim carbon atoms [13]. These reactions would provide positively charged PAH, which have been observed previously using mass spectrometry [15]. The clustering behaviour of $cPAH^+$ with other cPAH was beyond the scope of this publication but is worth considering in future work.

4. Conclusions

To conclude, we have demonstrated that for cPAH of the size found in early soot particles (≈15 rings with ≈2 pentagonal rings) are unable to invert at flame temperatures providing persistently polar species at flame temperatures. The transition from being easily inverted to becoming rigid at 1500 K for cPAH was found to be between 11 and 15 rings and often corresponded to a S-shaped transition state that was not stabilised by an increased aromaticity as with planar transition states. Π-radicals and chemi-ions were not found to influence the inversion barrier substantially with the number of pentagonal rings and total rings being of primary importance. *Ab initio* MD simulations were used to study the fluctuation of the dipole moment for molecule **4** at flame temperatures. The dipole moment was found to change on the timescale of the bending mode of the bowl, ≈300 fs, by ±10-20%. Some brief dynamics of the chemi-ion cPAH system were considered with the chemi-ion. An interaction with the pentagonal atoms with a flexoelectric effect was found as well as at the rim due to charge concentration. These results indicate that the polarity of cPAH found in early soot particles are important to consider in soot formation mechanisms.

Acknowledgements

This project was supported by the National Research Foundation (NRF), Prime Minister's Office, Singapore under its Campus for Research Excellence and Technological Enterprise (CREATE) programme. MK is grateful for the

support of the Alexander von Humboldt Foundation. All authors acknowledge the contributions of Prof. Hai Wang from Stanford University whose important comments initiated this work.

References

[1] H. Wang, Formation of nascent soot and other condensed-phase materials in flames, Proceedings of the Combustion Institute 33 (2011) 41–67.

[2] B. S. Haynes, H. G. Wagner, Soot formation, Progress in Energy and Combustion Science 7 (1981) 229–273.

[3] M. Frenklach, Reaction mechanism of soot formation in flames, Physical Chemistry Chemical Physics 4 (2002) 2028–2037.

[4] J. Happold, H.-H. Grotheer, M. Aigner, Soot precursors consisting of stacked pericondensed PAHs, in: Combustion generated fine carbonaceous particles, KIT Scientific Publishing, Karlsruhe, Germany, 2009, pp. 277–288.

[5] F. Carbone, M. R. Canagaratna, A. T. Lambe, J. T. Jayne, D. R. Worsnop, A. Gomez, Exploratory analysis of a sooting premixed flame via on-line high resolution (APi-TOF) mass spectrometry, Proceedings of the Combustion Institute 37 (2019) 919–926.

[6] M. Commodo, G. De Falco, A. Bruno, C. Borriello, P. Minutolo, A. D'Anna, Physicochemical evolution of nascent soot particles in a laminar premixed flame: From nucleation to early growth, Combustion and Flame 162 (2015) 3854–3863.

[7] M. L. Botero, E. M. Adkins, S. González-Calera, H. Miller, M. Kraft, PAH structure analysis of soot in a non-premixed flame using high-resolution transmission electron microscopy and optical band gap analysis, Combustion and Flame 164 (2016) 250–258.

[8] M. L. Botero, D. Chen, S. González-Calera, D. Jefferson, M. Kraft, HRTEM evaluation of soot particles produced by the non-premixed combustion of liquid fuels, Carbon 96 (2016) 459–473.

[9] M. Commodo, A. D'Anna, G. De Falco, R. Larciprete, P. Minutolo, Illuminating the earliest stages of the soot formation by photoemission and Raman spectroscopy, Combustion and Flame 181 (2017) 1339–1351.

[10] A. Faccinetto, P. Desgroux, M. Ziskind, E. Therssen, C. Focsa, High-sensitivity detection of polycyclic aromatic hydrocarbons adsorbed onto soot particles using laser desorption/laser ionization/time-of-flight mass spectrometry: An approach to studying the soot inception process in low-pressure flames, Combustion and Flame 158 (2011) 227–239.

[11] P. Desgroux, A. Faccinetto, X. Mercier, T. Mouton, D. Aubagnac Karkar, A. El Bakali, Comparative study of the soot formation process in a"nucleation" and a "sooting" low pressure premixed methane flame, Combustion and Flame 184 (2017) 153–166.

[12] T. S. Totton, A. J. Misquitta, M. Kraft, A quantitative study of the clustering of polycyclic aromatic hydrocarbons at high temperatures., Physical chemistry chemical physics 14 (2012) 4081–94.

[13] D. Chen, H. Wang, Cation-π interactions between flame chemi-ions and aromatic compounds, Energy & Fuels 31 (2017) 2345–2352.

[14] T. Baum, S. Löffler, P. Löffler, P. Weilmünster, K.-H. Homann, Fullerene ions and their relation to PAH and soot in low-pressure hydrocarbon flames, Berichte der Bunsengesellschaft für physikalische Chemie 96 (1992) 841–857.

[15] K. H. Homann, Fullerenes and soot formation - New pathways to large particles in flames, Angewandte Chemie, International Edition in English 37 (1998) 2435–2451.

[16] A. L. Lafleur, J. B. Howard, J. A. Marr, T. Yadav, Proposed fullerene precursor corannulene identified in flames both in the presence and absence of fullerene production, The Journal of Physical Chemistry 97 (1993) 13539–13543.

[17] X. Z. Wu, Y. R. Yao, M. M. Chen, H. R. Tian, J. Xiao, Y. Y. Xu, M. S. Lin, L. Abella, C. B. Tian, C.-L. Gao, Q. Zhang, S. Y. Xie, R. B. Huang, L. S. Zheng, Formation of curvature subunit of carbon in combustion, Journal of the American Chemical Society 138 (2016) 9629–9633.

[18] P. Gerhardt, S. Löffler, K. Homann, Polyhedral carbon ions in hydrocarbon flames, Chemical Physics Letters 137 (1987) 306 – 310.

[19] H. Richter, A. J. Labrocca, W. J. Grieco, K. Taghizadeh, A. L. Lafleur, J. B. Howard, Generation of higher fullerenes in flames, Journal of Physical Chemistry B 101 (1997) 1556–1560.

[20] R. D. Heidenreich, W. M. Hess, L. L. Ban, A test object and criteria for high resolution electron microscopy, Journal of Applied Crystallography 1 (1968) 1–19.

[21] R. L. Vander, A. Strzelec, T. J. Toops, C. S. Daw, C. L. Genzale, Forensics of soot : C5-related nanostructure as a diagnostic of in-cylinder chemistry, Fuel 113 (2013) 522–526.

[22] C. Wang, T. Huddle, C. H. Huang, W. Zhu, R. L. Vander Wal, E. H. Lester, J. P. Mathews, Improved quantification of curvature in high-resolution transmission electron microscopy lattice fringe micrographs of soots, Carbon 117 (2017) 174–181.

[23] J. W. Martin, M. Botero, R. I. Slavchov, K. Bowal, J. Akroyd, S. Mosbach, M. Kraft, Flexoelectricity and the Formation of Carbon Nanoparticles in Flames, The Journal of Physical Chemistry C 122 (2018) 22210–22215.

[24] M. L. Botero, Y. Sheng, J. Akroyd, J. Martin, J. A. Dreyer, W. Yang, M. Kraft, Internal structure of soot particles in a diffusion flame, Carbon 141 (2018) 635–642.

[25] M. Frenklach, L. B. Ebert, Comment on the proposed role of spheroidal carbon clusters in soot formation, The Journal of Physical Chemistry 92 (1988) 561–563.

[26] A. Violi, A. F. Sarofim, G. A. Voth, Kinetic Monte Carlo-molecular dynamics approach to model soot inception, Combustion Science and Technology 176 (2004) 991–1005.

[27] A. Violi, Cyclodehydrogenation reactions to cyclopentafused polycyclic aromatic hydrocarbons, Journal of Physical Chemistry A 109 (2005) 7781–7787.

[28] R. Whitesides, D. Domin, R. Salomón-Ferrer, W. A. Lester, M. Frenklach, Embedded-ring migration on graphene zigzag edge, Proceedings of the Combustion Institute 32 I (2009) 577–583.

[29] R. Whitesides, M. Frenklach, Detailed kinetic Monte Carlo simulations of graphene-edge growth., The Journal of Physical Chemistry. A 114 (2010) 689–703.

[30] R. Singh, M. Frenklach, A mechanistic study of the influence of graphene curvature on the rate of high-temperature oxidation by molecular oxygen, Carbon 101 (2016) 203–212.

[31] J. W. Martin, K. L. Bowal, A. Menon, R. I. Slavchov, J. Akroyd, S. Mosbach, M. Kraft, Polar curved polycyclic aromatic hydrocarbons in soot formation, Proceedings of the Combustion Institute 37 (2019) 1117–1123.

[32] J. W. Martin, R. I. Slavchov, E. K. Y. Yapp, J. Akroyd, S. Mosbach, M. Kraft, The polarization of polycyclic aromatic hydrocarbons curved by pentagon incorporation: the role of the flexoelectric dipole, The Journal of Physical Chemistry C 121 (2017) 27154–27163.

[33] H. F. Calcote, D. B. Olson, D. G. Keil, Are ions important in soot formation?, Energy & Fuels 2 (1988) 494–504.

[34] J. Lawton, F. Weinberg, Electrical aspects of combustion, Clarendon P., 1969.

[35] A. N. Hayhurst, H. R. N. Jones, Ions and soot in flames, Journal of the Chemical Society, Faraday Transactions 2 83 (1987) 1.

[36] A. Fialkov, Investigations on ions in flames, Progress in Energy and Combustion Science 23 (1997) 399–528.

[37] P. J. Mayo, F. J. Weinberg, On the size, charge and number-rate of formation of carbon particles in flames subjected to electric fields, Proceedings of the Royal Society A: Mathematical, Physical and Engineering Sciences 319 (1970) 351–371.

[38] M. Saito, T. Arai, M. Arai, Control of soot emitted from acetylene diffusion flames by applying an electric field, Combustion and Flame 119 (1999) 356–366.

[39] D. G. Park, B. C. Choi, M. S. Cha, S. H. Chung, Soot reduction under DC electric fields in counterflow non-premixed laminar ethylene flames, Combustion Science and Technology 186 (2014) 644–656.

[40] E. R. Place, F. J. Weinberg, Electrical control of flame carbon, Proceedings of the Royal Society A: Mathematical, Physical and Engineering Sciences 289 (1966) 192–205.

[41] S. Di Stasio, J. L. Legarrec, J. B. Mitchell, Synchrotron radiation studies of additives in combustion, II: Soot agglomerate microstructure change by alkali and alkaline-earth metal addition to a partially premixed flame, Energy and Fuels 25 (2011) 916–925.

[42] J. Simonsson, N. E. Olofsson, H. Bladh, M. Sanati, P. E. Bengtsson, Influence of potassium and iron chloride on the early stages of soot formation studied using imaging LII/ELS and TEM techniques, Proceedings of the Combustion Institute 36 (2017) 853–860.

[43] F. Carbone, S. Moslih, A. Gomez, Probing gas-to-particle transition in a moderately sooting atmospheric pressure ethylene/air laminar premixed flame. Part II: Molecular clusters and nascent soot particle size distributions, Combustion and Flame 181 (2017) 329–341.

[44] L. T. Scott, M. M. Hashemi, M. S. Bratcher, Corannulene bowl-to-bowl inversion is rapid at room temperature, Journal of the American Chemical Society 114 (1992) 1920–1921.

[45] T. J. Seiders, K. K. Baldridge, G. H. Grube, J. S. Siegel, Structure/energy correlation of bowl depth and inversion barrier in corannulene derivatives: Combined experimental and quantum mechanical analysis, Journal of the American Chemical Society 123 (2001) 517–525.

[46] C. H. Sun, G. Q. Lu, H. M. Cheng, Nonplanar distortions and strain energies of polycyclic aromatic hydrocarbons, Journal of Physical Chemistry B 110 (2006) 4563–4568.

[47] M. A. Dobrowolski, A. Ciesielski, M. K. Cyrański, On the aromatic stabilization of corannulene and coronene, Physical Chemistry Chemical Physics 13 (2011) 20557.

[48] A. H. Abdourazak, A. Sygula, P. W. Rabideau, "locking" the bowl-shaped geometry of corannulene: cyclopentacorannulene, Journal of the American Chemical Society 115 (1993) 3010–3011.

[49] T.-C. Wu, M.-K. Chen, Y.-W. Lee, M.-Y. Kuo, Y.-T. Wu, Bowl-Shaped Fragments of C_{70} or Higher Fullerenes: Synthesis, Structural Analysis, and Inversion Dynamics, Angewandte Chemie International Edition 52 (2013) 1289–1293.

[50] D. Hou, X. You, Reaction kinetics of hydrogen abstraction from polycyclic aromatic hydrocarbons by H atoms, Phys. Chem. Chem. Phys. 19 (2017) 30772–30780.

[51] J. R. Barker, Multiple-well, multiple-path unimolecular reaction systems. i. multiwell computer program suite, International Journal of Chemical Kinetics 33 (2001) 232–245.

[52] J. R. Barker, Energy transfer in master equation simulations: A new approach, International Journal of Chemical Kinetics 41 (2009) 748–763.

[53] J. Barker, T. Nguyen, J. Stanton, C. Aieta, M. Ceotto, F. Gabas, T. J. Kumar, C. Li, L. Lohr, A. Maranzana, N. Ortiz, J. Preses, J. Simmie, J. Sonk, P. Stimac, MultiWell-2017 Software Suite; J.R. Barker, University of Michigan, Ann Arbor, Michigan, USA, 2017.

[54] H. B. Schlegel, J. M. Millam, S. S. Iyengar, G. A. Voth, A. D. Daniels, G. E. Scuseria, M. J. Frisch, Ab initio molecular dynamics: Propagating the density matrix with Gaussian orbitals, The Journal of Chemical Physics 114 (2001) 9758–9763.

[55] S. S. Iyengar, H. B. Schlegel, J. M. Millam, G. A. Voth, G. E. Scuseria, M. J. Frisch, Ab initio molecular dynamics: Propagating the density matrix with Gaussian orbitals. II. Generalizations based on mass-weighting, idempotency, energy conservation and choice of initial conditions, Journal of Chemical Physics 115 (2001) 10291–10302.

[56] H. B. Schlegel, S. S. Iyengar, X. Li, J. M. Millam, G. A. Voth, G. E. Scuseria, M. J. Frisch, Ab initio molecular dynamics: Propagating the density matrix with Gaussian orbitals. III. Comparison with Born – Oppenheimer dynamics, The Journal of Chemical Physics 117 (2002) 8694–8704.

[57] X. Li, D. T. Moore, S. S. Iyengar, Insights from first principles molecular dynamics studies toward infrared multiple-photon and single-photon action spectroscopy: Case study of the proton-bound dimethyl ether dimer, The Journal of Chemical Physics 128 (2008) 184308.

[58] R. Das, P. K. Chattaraj, Gas storage potential of ExBox4+and its Li-decorated derivative, Physical Chemistry Chemical Physics 16 (2014) 21964–21979.

[59] L. Observatory, N. Bohrweg, N.-C. A. Leiden, Formation of Covalently Bonded Polycyclic Aromatic Hydrocarbons in the Interstellar Medium, The Astrophysical Journal 866 (2018) 113.

[60] C. A. Schuetz, M. Frenklach, Nucleation of soot: Molecular dynamics simulations of pyrene dimerization, Proceedings of the Combustion Institute 29 (2002) 2307–2314.

[61] D. Wong, R. Whitesides, C. Schuetz, M. Frenklach, Molecular dynamics simulations of PAH dimerization, in: Combustion Generated Fine Carbonaceous Particles, KIT Scientific Publishing Karlsruhe, 2009, pp. 247–257.

[62] S. Grimme, Semiempirical GGA-type density functional constructed with a long-range dispersion correction, Journal of Computational Chemistry 27 (2006) 1787–1799.

[63] T. Janowski, P. Pulay, A. A. Sasith Karunarathna, A. Sygula, S. Saebø, Convex-concave stacking of curved conjugated networks: Benchmark calculations on the corannulene dimer, Chemical Physics Letters 512 (2011) 155–160.

[64] A. R. Neves, P. A. Fernandes, M. J. Ramos, The accuracy of density functional theory in the description of cation-π and π-hydrogen bond interactions, Journal of Chemical Theory and Computation 7 (2011) 2059–2067.

[65] M. J. Frisch, G. W. Trucks, H. B. Schlegel, G. E. Scuseria, M. A. Robb, J. R. Cheeseman, G. Scalmani, V. Barone, G. A. Petersson, H. Nakatsuji, X. Li, M. Caricato, A. V. Marenich, J. Bloino, B. G. Janesko, R. Gomperts, B. Mennucci, H. P. Hratchian, J. V. Ortiz, A. F. Izmaylov,

J. L. Sonnenberg, D. Williams-Young, F. Ding, F. Lipparini, F. Egidi, J. Goings, B. Peng, A. Petrone, T. Henderson, D. Ranasinghe, V. G. Zakrzewski, J. Gao, N. Rega, G. Zheng, W. Liang, M. Hada, M. Ehara, K. Toyota, R. Fukuda, J. Hasegawa, M. Ishida, T. Nakajima, Y. Honda, O. Kitao, H. Nakai, T. Vreven, K. Throssell, J. A. Montgomery, Jr., J. E. Peralta, F. Ogliaro, M. J. Bearpark, J. J. Heyd, E. N. Brothers, K. N. Kudin, V. N. Staroverov, T. A. Keith, R. Kobayashi, J. Normand, K. Raghavachari, A. P. Rendell, J. C. Burant, S. S. Iyengar, J. Tomasi, M. Cossi, J. M. Millam, M. Klene, C. Adamo, R. Cammi, J. W. Ochterski, R. L. Martin, K. Morokuma, O. Farkas, J. B. Foresman, D. J. Fox, Gaussian 16 Revision B.01, 2016. Gaussian Inc. Wallingford CT.

[66] P. U. Biedermann, S. Pogodin, I. Agranat, Inversion barrier of corannulene. a benchmark for bowl-to-bowl inversions in fullerene fragments, The Journal of Organic Chemistry 64 (1999) 3655–3662.

[67] M.-k. Chen, H.-j. Hsin, T.-c. Wu, B.-y. Kang, Y.-w. Lee, M.-Y. Kuo, Y.-T. Wu, Highly Curved Bowl-Shaped Fragments of Fullerenes: Synthesis, Structural Analysis, and Physical Properties, Chemistry - A European Journal 20 (2014) 598–608.

[68] E. K. Yapp, C. G. Wells, J. Akroyd, S. Mosbach, R. Xu, M. Kraft, Modelling PAH curvature in laminar premixed flames using a detailed population balance model, Combustion and Flame 176 (2017) 172–180.

[69] J. S. Chickos, P. Webb, G. Nichols, T. Kiyobayashi, P.-C. Cheng, L. Scott, The enthalpy of vaporization and sublimation of corannulene, coronene, and perylene at T= 298.15 K, The Journal of Chemical Thermodynamics 34 (2002) 1195–1206.

[70] A. Karton, Inversion and rotation processes involving non-planar aromatic compounds catalyzed by extended polycyclic aromatic hydrocarbons, Chemical Physics Letters 614 (2014) 156–161.

[71] P. A. Denis, Pristine graphene-based catalysis: Significant reduction of the inversion barriers of adsorbed and confined corannulene, sumanene, and dibenzo[a, g]corannulene, Journal of Physical Chemistry A 119 (2015) 5770–5777.

[72] M. Juríček, N. L. Strutt, J. C. Barnes, A. M. Butterfield, E. J. Dale, K. K. Baldridge, J. F. Stoddart, J. S. Siegel, Induced-fit catalysis of corannulene bowl-to-bowl inversion, Nature Chemistry 6 (2014) 222–228.

[73] J. W. Martin, G. J. McIntosh, R. Arul, R. N. Oosterbeek, M. Kraft, T. Söhnel, Giant fullerene formation through thermal treatment of fullerene soot, Carbon 125 (2017) 132–138.